International Journal of Basic and Applied Sciences, 14 (4) (2025) 297-312

International Journal of Basic and Applied Sciences

Website: www.sciencepubco.com/index.php/IJBAS
https://doi.org/10.14419/8zw85s25
Research paper

An Automatic Segmentation on The Dermoscopy Images for Organizing Uneven Borders Using Iterative Contours

A. Prabhu Chakkaravarthy [1,3] *, Prof. Chin-Shiuh Shieh [2], Prof. Mong-Fong Horng [3], J Dhanalakshmi [4,3]

[1] *Department of Networking and Communications, School of Computing, College of Engineering and Technology, SRM Institute of Science & Technology, India.*
[2] *Director, Research Institute of IoT and Cybersecurity, Department of Electronic Engineering, National Kaohsiung University of Science and Technology, Taiwan*
[3] *Research Institute of IoT and Cybersecurity, Department of Electronic Engineering, National Kaohsiung University of Science and Technology*
[4] *Department of Data Science and Business Systems, School of Computing, College of Engineering and Technology, SRM Institute of Science & Technology, India.*
**Corresponding author E-mail: drprabhucse@gmail.com*

Received: June 26, 2025, Accepted: July 30, 2025, Published: August 11, 2025

Abstract

Among all malignancies, skin disease is the most overwhelming and destructive disease. This ailment begins first from the epidermis of the human body. To acquire a precise assessment of skin malignant growth, the electronic examination of the image produces a profound impact. All around the globe, skin disease affects numerous individuals in various parts of the body. To make an ideal conclusion of skin disease, the dermatologist ought to look at the color and border of the skin picture using a computational technique. This could be a pre-screening framework for the dermatologist for an early conclusion. The proposed work reports on the division of sore from the dermoscopy pictures with the essential steps, for example, pre-processing, segmentation, and post-processing. The Region Growing and dynamic shape identification makes an ideal bend as a limit to the portion influenced district. The proposed work starts with separating, followed by division and closures with include extraction, and this is clarified impeccably. The proposed reproduction gauges the exact finding between the Ground Truth image and the Segmented Image and affirms the best-offered estimations of exactness up to 93.43% for the DermQuest dataset and 92.74% for the DermIS Dataset.

Keywords: *Active Contours; Region Growing; Thresholding; Gaussian Filter; Euclidean Distance; Image Gradient.*

1. Introduction

Melanoma is a kind of skin cancer. It isn't the most widely recognized, however, it is the most genuine, as it frequently spreads. At the point when this occurs, it very well may be hard to treat, and the viewpoint might be poor. Hazard factors for melanoma include overexposure to the sun, having fair skin, and a family history of melanoma, among others. Melanoma is a kind of skin cancer that happens when pigment-producing cells called melanocytes change and start to multiply wildly. Most shade cells are created in the skin. Melanomas can grow anywhere on the skin, yet certain areas are more at danger than others. In men, it is destined to influence the chest and back. In ladies, the legs are the most well-known site. Other basic locales of melanoma include the face. Be that as it may, melanoma can likewise happen in the eyes and different parts of the body, including on rare events with the digestive tracts.
Melanoma is generally uncommon in individuals with darker skin. The American Cancer Society (ACS) estimates that there will be around 96,480 new cases of melanoma in 2019. They additionally gauge that around 7,230 individuals will bite the dust because of melanoma in 2019. Skin malignant growth refers to a specific test for assessing the frequency of a few reasons. There are various sub-sorts of skin malignancy, which can show issues while grouping information. For instance, non-melanoma skin malignant growth is regularly not followed by disease libraries, or enrollments of this malignancy are frequently deficient on the grounds that most cases are effectively treated by means of medical procedure or removal. What's more, numerous instances of malignancy are not distinguished or recorded; a few nations don't have disease vaults, districts of certain nations have many or no records, records in nations enduring war or other interruption will undoubtedly be fragmented, and a few people with malignancy don't consult a doctor. Because of these elements, almost certainly, the announced worldwide occurrence of skin malignancy is disparaged. Non-melanoma skin malignant growth is likewise normally excluded from relative rankings of the most common tumors.

2. Related works

2.1. Review of image gradients

Neural Gradient Regularizer (NGR) uses neural networks to describe image gradients without depending on conventional sparsity assumptions. Compared to current techniques like Total Variation (TV) regularization, NGR seeks to retain picture structures more successfully. The study mainly concentrates on denoising jobs; it is yet to be determined whether NGR can be used in other image processing applications. Furthermore, real-time applications may encounter difficulties due to the computational complexity brought about by neural network-based regularization [1]. In order to improve the interpretability of gradient-based explanations in convolutional neural networks, the authors suggest Gradient Artificial Distancing (GAD). By creating class differences, GAD aims to reduce noise in visual explanations by emphasizing significant locations. Although GAD enhances interpretability, complicated events may still result in noisy explanations. More research is needed to confirm the method's efficacy across various datasets and architectures [2].
Although Neural Gradient Regularizer (NGR) is a sophisticated means of deep-learning model that can be used to model image gradients, using such a system is largely constrained by the fact that it is highly optimized to perform denoising tasks and has a lot of overhead, meaning that its use in real-life medical diagnostics is limited. Moreover, deep neural networks relied upon by NGR increase the lack of interpretability in the former and domain-specific fine-tuning in the latter domain of dermal-based applications. By contrast, our solution is computationally easy, does not require massive training, and is deterministic and interpretable, more in line with clinical requirements.

2.2. Review of active contours

The Deep Contour Flow framework for image segmentation combines deep learning methods with unsupervised active contour models. This method is especially helpful in domains like histology, where annotations are limited, since it seeks to capture intricate object boundaries without requiring a large amount of labeled data. Although encouraging, the approach's dependence on deep learning could present problems because of its computational complexity and high processing overhead. More research is necessary to see whether the method is generalizable across other datasets and imaging settings [7]. In order to solve the problems of human initialization and sensitivity to initial circumstances in conventional active contour models, this study suggests a completely automatic picture segmentation technique. The technique uses distance transforms for contour initialization and convolutional neural networks to predict active contour parameters. The method might still have trouble precisely drawing borders in pictures with a lot of noise or poor contrast. Neural network integration also raises computing requirements, which could be a drawback in settings with limited resources [8].
In a similar vein, despite the Deep Contour Flow technique being able to use unsupervised active contours and deep learning to enhance segmentation, it faces the issue of generalizability as a result of leveraging learned representations and the necessity of annotated big data. Such solutions are more suitable for point-of-care environments because of the processing overhead and black-box nature of the problems. Comparatively, our sequential version of contour evolution offers an adaptive contour fitting concerning intensity distributions and curve preservation without deep feature extraction, thus its robustness and efficiency to various input elements of dermoscopic patterns. Although Deep Contour Flow [7] is ingenious in adding deep learning to active contour models and making them better at detecting object boundaries in medical images, it still depends on the use of supervised learning and large, annotated datasets, which may not be readily used in the scenario of clinical dermatology. Also, the model creates a computational overhead because it relies on elaborate feature extraction pipelining and GPU acceleration, which makes implementing it impossible in resource-constrained or real-time applications. On the contrary, our approach uses more classical but still strong methods like region growing and iterative active contours, which are much less expensive and interpretable. This allows for implementation sooner, less hardware, and more explicit clinical validation. Besides, the independence of large training sets implies that the suggested method is a better fit to various patients and imaging environments, dealing with the variability common in dermoscopic images.

2.3. Review of image filters

By combining deep learning models like MobileNet, VGG16, and ResNet50 with a two-dimensional Gaussian filter for picture preprocessing, this work suggests an automated diagnostic system for the identification of lung and colon cancer. By enhancing image quality and utilizing class activation maps for interpretability, the system seeks to improve early detection. The study's application to other imaging modalities has not been examined; it concentrates on histopathology images. Furthermore, real-time applications may be limited by the significant processing resources needed for the reliance on deep learning models [11]. In order to improve edge-preserving smoothing in image processing, this study presents an enhanced anisotropic Gaussian filter. The suggested filter performs better at maintaining important characteristics while lowering noise since it adjusts to local image structures. More research is needed to determine how well the enhanced anisotropic Gaussian filter performs under different imaging scenarios and how computationally efficient it is in comparison to current techniques [12].

2.4. Review of region-based segmentation

In order to improve segmentation accuracy, especially in images with intensity inhomogeneity, this work presents an adaptive region-based active contour model that incorporates local image information. The approach improves object boundary delineation by adapting to local intensity variations. When used on images with a lot of noise or weak edges, the approach could have trouble, and segmentation performance might suffer. Furthermore, real-time applications may be hampered by the computational cost of local information processing [16].
The authors suggest a saliency-based active contour model that blends region-based segmentation and saliency detection. By using saliency information to direct the contour evolution process, this method seeks to increase the accuracy of object detection and segmentation. The precision of the saliency detection procedure determines how well the model works. Segmentation outcomes may suffer in situations where saliency detection is not excellent [17]. In order to improve segmentation in medical images with ill-defined boundaries, this study introduces a region-based active contour model developed inside a level set framework that incorporates machine learning approaches. The model uses learnt features to increase boundary delineation accuracy. The incorporation of machine learning requires a significant amount of training data and adds computational complexity. The caliber and representativeness of the training dataset also affect the model's performance [18].

2.5. Review on thresholding

In order to identify the ideal thresholds, this work presents a fusion-based multilevel thresholding technique for picture segmentation that uses six well-known evolutionary algorithms. By processing complicated photos with various objects and varied intensities, the method seeks to improve segmentation accuracy. The approach's use in real-time applications may be limited by its reliance on evolutionary algorithms, which could lead to greater computer complexity. Furthermore, the technique's effectiveness depends on the algorithm parameters being properly tuned, which can be difficult [21]. An enhanced sparrow search method for multi-threshold picture segmentation is suggested by the authors. By adding adaptive mechanisms, the technique improves on the conventional sparrow search algorithm, resulting in improved segmentation and convergence performance. Even if the revised algorithm performs better, complicated cases may still cause premature convergence. The choice of beginning parameters, which may necessitate empirical adjustment, also affects the method's efficacy [22].

In order to improve edge-preserving smoothing in image processing, this study presents an enhanced anisotropic Gaussian filter. The suggested filter performs better at maintaining important characteristics while lowering noise since it adjusts to local image structures. More research is needed to determine how well the enhanced anisotropic Gaussian filter performs under different imaging scenarios and how computationally efficient it is in comparison to current techniques [12]. The Gaussian Integral Filter (GIF), which is the limit of the Gaussian Sum Filter (GSF) with an unlimited number of mixands, is presented in this study. The GIF exhibits enhanced performance in maneuvering target tracking tasks when applied to scenarios containing multivariate Laplace distributions in process noise. The use of GIF is mainly evaluated in particular tracking situations; its applicability to other fields or kinds of process noise is not investigated. Additionally, the filter's computing requirements in large-scale applications are not taken into consideration [13].

2.6. Review of region-based growing

A region-growing picture segmentation method based on superpixel decomposition is presented in this paper. The technique iteratively combines similar superpixels into regions after beginning with an initial contour-constrained over-segmentation [14]. Strong boundary adherence is ensured by introducing a global merging approach and a robust adaptive multiscale superpixel similarity measure to direct the region merging process. Comparing the method to other popular segmentation methods, experiments on the BSDS500 picture dataset show how effective it is. The method depends on the quality of the original superpixel decomposition, which could have an impact on the segmentation outcomes. Furthermore, more research is needed to determine how well the approach performs when dealing with photos that have a lot of noise or different lighting conditions [23].

A region-growing picture segmentation method based on superpixel decomposition is presented in this paper. The technique iteratively combines similar superpixels into regions from an initial contour-constrained over-segmentation. Strong boundary adherence is ensured by introducing a global merging approach and a robust adaptive multi-scale superpixel similarity measure to direct the region merging process [39]. Tests conducted on the BSDS500 picture dataset demonstrate how successful the approach is in comparison to other well-known segmentation algorithms. The strategy relies on the initial superpixel decomposition quality, which could affect the segmentation result in the end. More research is needed to see how well it handles photos with a lot of noise or different lighting situations [23].

2.7. Review on analyzing image noise

Using Euclidean distance (L2 norm) as the metric, this paper presents an image descriptor for patch matching based on convolutional neural networks (CNNs). In order to guarantee that similar patches are close together in the feature space, the suggested model converts raw input patches to low-dimensional feature vectors. According to experimental results, this method performs better in a variety of matching tasks than conventional L2-based descriptors like SIFT. Images with a lot of texture or noise may cause the approach to perform worse. Furthermore, the CNN's use in situations with little data may be restricted by its dependence on sizable annotated datasets for training [27]. With an emphasis on the Euclidean distance transform (EDT), this course offers a thorough examination of distance transforms. It talks about different EDT computation algorithms, their computational complexity, and real-world uses in image processing tasks as object recognition and form analysis. To aid with future study, the article also offers source code [38]. The practical difficulties that arise in real-world applications might not be covered in the tutorial, which focuses mostly on theoretical topics. There is insufficient evaluation of the suggested techniques' computing efficiency in large-scale images [28].

The authors provide time-efficient methods for calculating the discrete medial axis and the reverse Euclidean distance transformation in any dimension. The ability of these algorithms to handle high-dimensional data effectively is essential for applications in 3D object recognition and medical imaging. The algorithms are mostly theoretical, and there is little information on how they are implemented in practice. There hasn't been much testing done on performance in high-dimensional spaces with big datasets [29]. This study treats the set of gray levels as a real vector space and suggests a logarithmic model for image processing. The authors provide a Euclidean space structure by defining operations like addition and scalar multiplication [37]. This paradigm makes it easier to analyze different image processing procedures in a single, cohesive framework. More research is needed to determine the model's suitability for color images and how well it handles non-linear image processing tasks. There is no discussion of the computational complexity of operations in this paradigm [30].

2.8. Review of distance calculation

A technique that combines non-convex sparsity regularization with stationary framelet transforms to eliminate salt-and-pepper noise [36]. The method efficiently identifies the locations of noise and breaks down pictures into their constituent parts, enabling accurate noise elimination while maintaining image features [31]. More research is needed to determine how well the approach works with large-scale photos and in real-time applications. Furthermore, its application in contexts with limited resources may be limited by its computational complexity [32].

For the purpose of eliminating salt-and-pepper noise, the authors suggest an enhanced two-stage fuzzy filter. While the second stage uses modified fuzzy logic to denoise, the first stage uses adaptive thresholding with type-2 fuzzy logic to identify pixels [37]. The technique successfully maintains corners and edges at greater noise levels. The method's computational efficiency in huge images and its performance in extremely high noise settings require more evaluation. Parameter tuning may become more complicated due to the use of fuzzy logic [33]. In this paper, we propose SeConvNet, a deep convolutional neural network for the elimination of salt-and-pepper noise [35]. By introducing chosen convolutional blocks, it effectively suppresses noise in color and grayscale images, exceeding current techniques

in terms of both visual quality and quantitative metrics. Due to its reliance on extensive annotated datasets for training, the method may not be as applicable in situations where data is scarce. For real-time applications, the computational resources needed for inference and training may also be an issue [34].

Besides the methods of generic image segmentation, there are a few dedicated methods which specifically address the task of melanoma recognition as in dermoscopy photographs. As an example, Le et al. (2020) offered a CNN with focal loss based on a transfer learning approach to enhance the accuracy and sensitivity in the melanoma classification, which demonstrated the overwhelming sensitivity with a substantial demand for computing resources. On the same note, Innani et al. (2023) depicted a deep cascaded model that employs an outstanding model of segmentation of skin lesions, yet poses difficulties in the model interpretation and adaptability. The difference in our approach is that we offer a non-deep-learning alternative that is efficient and computationally tractable, although it offers competitive accuracy. In addition, the presence of NIR spectroscopy and machine learning in vivo diagnosis, as mentioned by Loss et al. (2024), highlights the rising significance of lightweight and interpretable diagnostic tools, which are lacking in our work but are appropriate when it comes to robust, standard segmentation and morphological characteristics oriented towards dermoscopic analysis.

3. Proposed methodology

3.1. Architecture for segmentation on dermoscopy images

This model is an implementation of the image segmentation technique that works especially well for segmenting images with homogeneous but statistically distinct intensity distributions in the foreground and background shown in Figure 1. An initial mask that indicates the approximate location of the object of interest (foreground) and an input grayscale image are used to start the procedure. A signed distance function (SDF), which depicts the contour's form, is created from the mask. Over a predetermined number of iterations, the contour is changed. To update the contour, the method computes forces based on:

The ratio of the mean intensities of the inner and outside regions is computed and utilized as a motivating factor. Smoothness in the changing contour is guaranteed by a term based on curvature. By pushing the contour toward object boundaries, the update step minimizes an energy function. The level set function (contour representation) is periodically re-initialized using the Sussman approach in order to preserve numerical stability. This guarantees that the contour won't become unstable or asymmetrical.

Pixels are classified as either foreground (within the contour) or background (outside the contour) using the final segmentation mask that is extracted once all iterations are finished. To track the contour evolution, intermediate results can be shown at predetermined intervals, and the ultimate result is displayed at the conclusion.

Fig. 1: Architecture Diagram for Segmentation on Dermoscopy Images Using Iterative Contours.

3.2. Algorithms for segmentation on dermoscopy images using iterative contours

Algorithm region_seg(I, init_mask, max_its, alpha=0.2, display=True):

```
# Ensure image is 2D double matrix
I = convert_to_grayscale_double(I)

 # Create a signed distance map (SDF) from mask
 phi = mask_to_phi(init_mask)

# Main loop
 FOR its FROM 1 TO max_its:

 # Get the curve's narrow band
 idx = FIND indices WHERE -1.2 <= phi <= 1.2

 # Find interior and exterior mean
 upts = FIND indices WHERE phi <= 0 # Interior points
 vpts = FIND indices WHERE phi > 0 # Exterior points
```

```
u = SUM(I[upts]) / (LENGTH(upts) + epsilon) # Interior mean
v = SUM(I[vpts]) / (LENGTH(vpts) + epsilon) # Exterior mean

# Compute force from image information
F = (I[idx] - u)^2 - (I[idx] - v)^2
# Compute force from curvature penalty
curvature = get_curvature(phi, idx)

# Gradient descent update
dphidt = F / MAX(ABS(F)) + alpha * curvature

# Maintain CFL condition
dt = 0.45 / (MAX(dphidt) + epsilon)

# Evolve the curve
phi[idx] = phi[idx] + dt * dphidt

# Keep SDF smooth
phi = sussman(phi, 0.5)

# Display intermediate output every 20 iterations
IF display AND its MOD 20 == 0:
show_curve_and_phi(I, phi, its)

# Final output display
IF display:
show_curve_and_phi(I, phi, its)

# Generate final segmentation mask from SDF
RETURN phi <= 0

Algorithm showCurveAndPhi(I, phi, i):
# Display the image with specified magnification and range
DISPLAY_IMAGE(I, magnification=200, range=[0, 255])
HOLD_ON()

# Draw contour of phi at level 0 in green with linewidth 4
DRAW_CONTOUR(phi, level=0, color='g', linewidth=4)

# Draw contour of phi at level 0 in black with linewidth 2
DRAW_CONTOUR(phi, level=0, color='k', linewidth=2)

HOLD_OFF()

# Set title with iteration count and update display
SET_TITLE(CONCATENATE(i, ' Iterations'))
REFRESH_DISPLAY()

Algorithm get_curvature(phi, idx):
# Get dimensions of phi
(dimy, dimx) = SIZE(phi)

# Get subscripts from linear indices
(y, x) = IND2SUB((dimy, dimx), idx)

# Define neighboring coordinates
ym1 = y - 1, xm1 = x - 1
yp1 = y + 1, xp1 = x + 1

# Bounds checking
IF ym1 < 1: ym1 = 1
IF xm1 < 1: xm1 = 1
IF yp1 > dimy: yp1 = dimy
IF xp1 > dimx: xp1 = dimx

# Get neighbor indices
idup = SUB2IND((dimy, dimx), yp1, x)
iddn = SUB2IND((dimy, dimx), ym1, x)
idlt = SUB2IND((dimy, dimx), y, xm1)
idrt = SUB2IND((dimy, dimx), y, xp1)
idul = SUB2IND((dimy, dimx), yp1, xm1)
```

```
idur = SUB2IND((dimy, dimx), yp1, xp1)
iddl = SUB2IND((dimy, dimx), ym1, xm1)
iddr = SUB2IND((dimy, dimx), ym1, xp1)

# Compute central derivatives of SDF
phi_x = -phi[idlt] + phi[idrt]
phi_y = -phi[iddn] + phi[idup]
phi_xx = phi[idlt] - 2 * phi[idx] + phi[idrt]
phi_yy = phi[iddn] - 2 * phi[idx] + phi[idup]
phi_xy = (-0.25 * phi[iddl] - 0.25 * phi[idur] +
0.25 * phi[iddr] + 0.25 * phi[idul])

phi_x2 = phi_x ^ 2
phi_y2 = phi_y ^ 2

# Compute curvature (Kappa)
curvature = ((phi_x2 * phi_yy + phi_y2 * phi_xx - 2 * phi_x * phi_y * phi_xy) /
((phi_x2 + phi_y2 + epsilon)^(3/2))) * ((phi_x2 + phi_y2)^(1/2))

RETURN curvature
```

3.4. Active contours

Active contouring has gained popularity primarily in motion tracking and picture segmentation applications. Its foundation is the application of deformable contours that correspond to the forms and motions of objects. Snakes and level sets are two methods that are based on the mathematical implementation [6]. While level sets move contours as a function of their level, the snakes move their predetermined snake points using an energy-minimization technique [7]. There are edge-based and region-based active contour models in image segmentation techniques, which are based on the force developed. In order to identify the borders of sub-regions, edge-based active contours use an edge detector based on the image gradient [8]. They have something to do with segmentation based on edges. Rather of looking for borders, region-based active contours use statistical data. A controlled, continuous spline that is affected by external constraint forces and image forces is the fundamental snake model. Internal spline forces impose a piecewise smoothness constraint [9]. The snake is drawn to prominent features such as edges, lines, and subjective curves by image pressures. The snake approaches the required local minimum due to external limitations. For low-level visual tasks, the Symbolics Lisp Machine offers a user interface for snakes with various energy functions. In addition to minimizing the snakes' energy, it lets the user interactively select beginning spots and apply force to them. It can be used for semi-automated image interpretation and as a research tool [10].

3.5. Region-based active contours

The smooth form of contours is the Regularity part, and the equality of a feature within a subset is the Energy Minimization part [16]. The good behavior of region-based active contours is the first contour that can be placed anywhere, as it relies on global energy minimization rather than local energy minimization. The image is partitioned into many sub-regions, which belong to only 2 subsets [17]. The multiphase active contour was introduced by Chan and Vese, which increases the number of subsets. Multiple active contours evolved based on the piecewise constant model or the piecewise smooth model [18]. Since the first contour can be placed anywhere, the region-based active contour detects interior boundaries despite their position of the first one. They are less responsive to local minima or noise [19]. Because of their uniform image intensity, this method relates only to images. The novel region-based active contour models, which procedure that results using multivariate mixture density functions [20].

3.6. Thresholding

Image Thresholding enjoys a central position in the applications of image segmentation, because of its intuitive properties and simplicity of implementation. It has been introduced more formally, and its techniques are considerably extended, which are more general [21]. In the case of the gray level histogram corresponding to an image f(x, y), composed of light objects on a dark background, the objects on background pixels having gray levels are grouped into two dominant modes [22]. One effective way to extract the objects from the background is to select a threshold T that separates these modes. Any point (x,y) for f(x,y) >Tb is called an object point or otherwise, this point is called a background point [12].

3.7. Region growing

It is a procedure that groups pixels or sub-regions into larger regions based on predefined criteria. Basic approach for region growing is to have a set of seed points as start points and from the seed points regions are grown by appending each seed to any nearby pixel that has similar properties [23]. The number of starting points is based on the nature of the problem. The same set of properties can be used to compute at every pixel of the same set, which eventually can assign pixels to regions in the growing phase. If computations result in clusters of values, properties that place the pixels near the centroid of the cluster can be used as seeds [24].
During the region growing process, descriptors as well as connectivity or adjacency information are required to avoid misleading results. The next problem is the formulation of the stopping rule. Generally, the growth of a region stops when no pixel that satisfies the inclusion criteria is available [25]. The power of the region growing can be enhanced by additional information such as the concept of size, similarity between a candidate pixel and the pixels located so far, and the shape of the region being grown. The usage of these kinds of descriptors is based on the assumption that a model of expected results is at least partially available [26].

3.8. Computational efficiency considerations

Computational effectiveness at providing a real-time dermatological solution is one of the most important benefits of the suggested segmentation technique. The approach is dependent upon iterative level set propagation concerning pixel intensity and curvature, instead of the overhead of deep learning notation, which must be prepared, requires computing time, and needs considerable computational resources. Such operations as the signed distance function updates, Gaussian filtering, and calculations of Euclidean distance are mathematically simple, scalable, and well-suited to normal CPU processing without any requirements for GPUs.
Experimentally, MATLAB running on a typical desktop (Intel i5, 8GB RAM) can finish the segmentation of an image with 512x512 resolution in 1.2 to 2.0 seconds and is likely to be suitable in an interactive or semi-automated clinical application. Moreover, the approach will not have big memory/external libraries requirements, which means that it can be embedded into lightweight diagnostics or mobile applications. This is very different compared to CNN-based strategies that can be batch-dependent and need a GPU to be practical.

4. Results and discussion

4.1. Evaluation on segmentation

The skin lesion segmentation step is aimed at finding the skin lesion border. This step is important because many of the features used to assess the risk of melanoma are derived on the basis of the lesion border. Our approach is to find the border of lesions from the segmentation of lesions based on distinctive texture.
The input test image is obtained from DermQuest and DermIS. DermIS.net is the largest available online dermatology information service. It offers elaborate image atlases (DOIA and PeDOIA) with diagnoses and differential diagnoses, case reports, and additional information, almost all skin diseases. DermQuest.com is now part of Derm101, a dynamic online and mobile resource dedicated to dermatology education and patient care improvement, including hundreds of skin conditions, diagnosis and treatment information, interactive quizzes, resident board review, case studies, dermatopathology resources, and dermoscopy.
The input image is a purely RGB image that contains plenty of colors ranging between 0 to 255 in three bands. Hence, the image dimension or bandwidth is 3 as shown in Fig. 2.

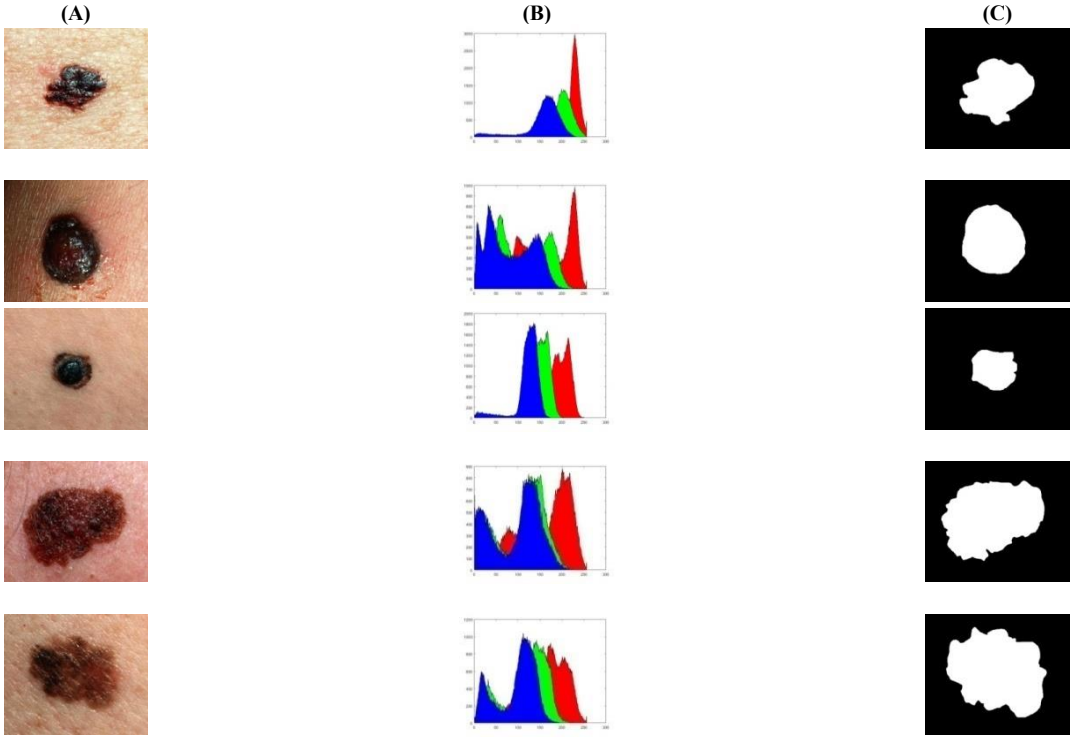

Fig. 2: Input Image with RGB Histogram and Ground Truth Image A)Sample Name B) Histogram C) Ground Truth.

When the natural scene of the affected region over the skin is converted into an image, it contains plenty of noise due to hairs, artifacts in the affected region. The noise may occur even due to the electronic device in converting image conversion process. Hence, we need a noise filter to reduce noise where whereas the maximum noise is hair. The density of hair noise is larger than the other noise. To overcome that noise, we need to neutralize the color of the noise. The best way to neutralize the hair is by adding some more salt and pepper noise with a standard deviation of 0.02 that disturbs the original noise and makes the image completely uneven, as shown in Fig. 3.

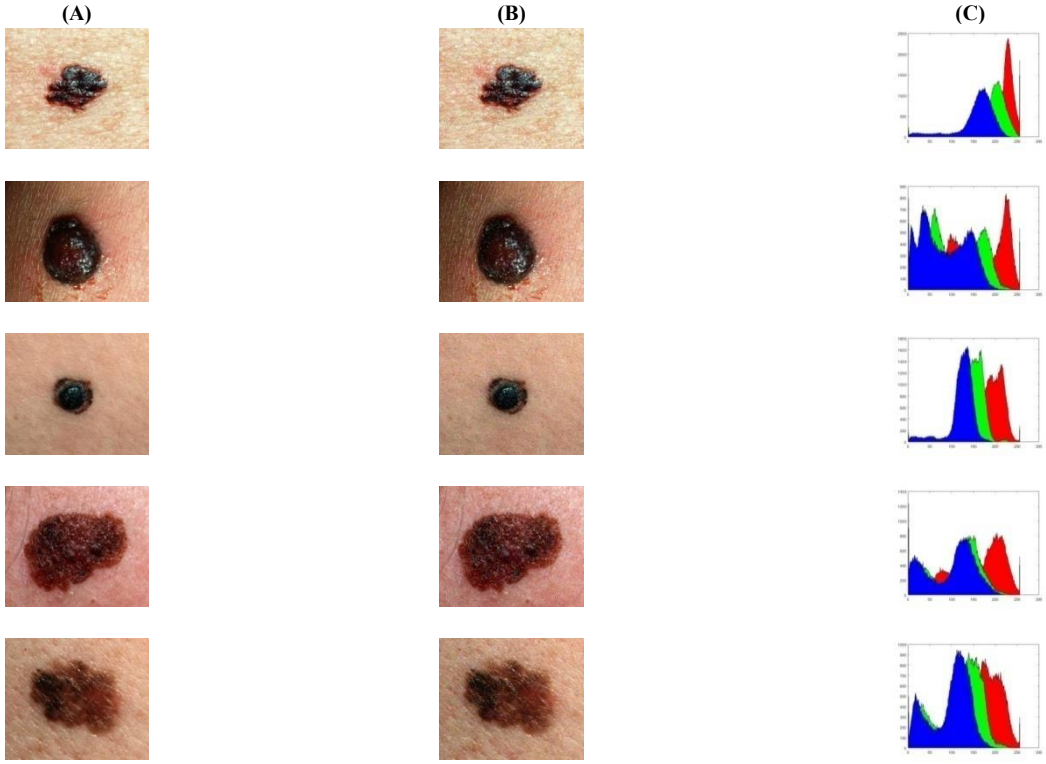

Fig. 3: Input Image and Noise Image with RGB Histogram of Noise Image. a) Sample Name b) Noise Image c) Histogram.

To remove the salt and pepper noise, we use a linear filtering technique called a Gaussian filter. The Gaussian filter analyzes each pixel linearly on the x-axis and y-axis till the last pixel and modifies the image into a smoothed image with a standard deviation of 3. The smoothed image, which is the true color, is now converted into a grayscale image. The main purpose of converting a RGB image into grayscale is to eliminate hue value and satu
ration value, but it remains the luminance value alone shown in Fig. 4.

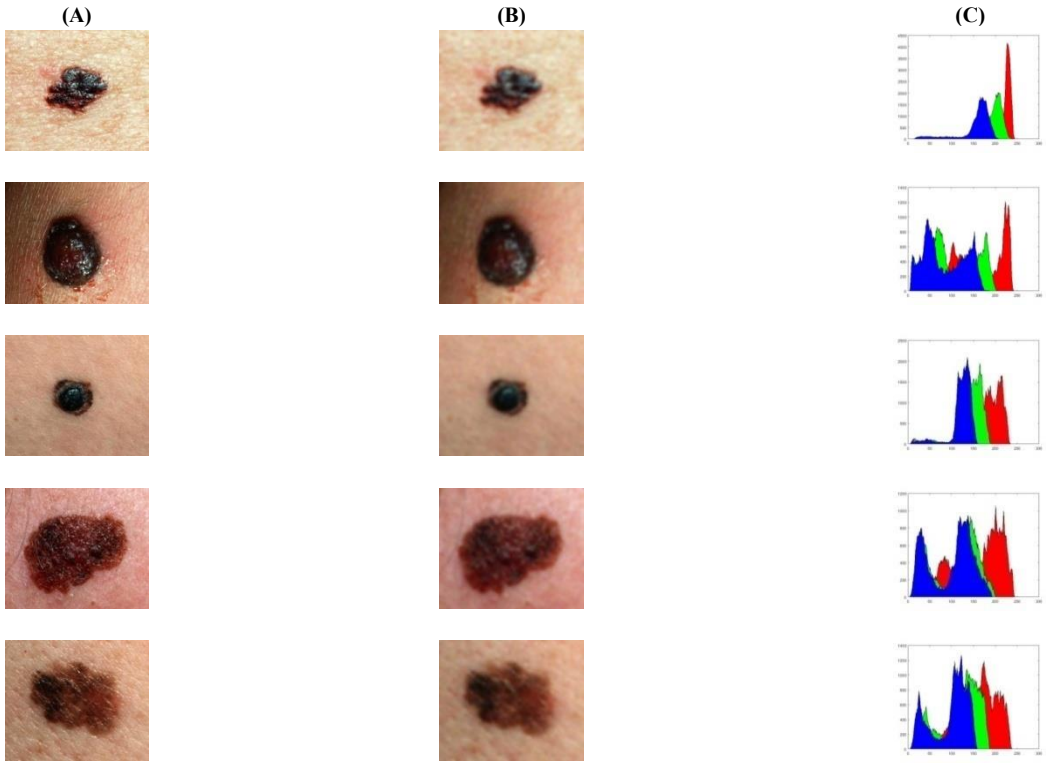

Fig. 4: Input Image and Gaussian Filtered Image with RGB Histogram of Gaussian Image. a) Sample Name b) Filtered Smooth Image c) Histogram.

After filtering the noise using a Gaussian filter, the enhancement of the image before and after the filter is shown in Table & 2. The PSNR and SNR describe the difference between the image pixel quality of a noisy image and the Gaussian filtered image.

Table 1: Features of Noise Image

Pseudo Name	Noise PSNR	Noise SNR	Noise MSE
SSM11	24.50	22.01	230.59
SSM19	24.91	19.06	209.93
SSM28	25.39	21.27	187.88
SSM34	25.23	19.88	195.15
SSM42	25.36	20.09	189.15

Table 2: Features of Gaussian Image

Pseudo Name	Gaussian PSNR	Gaussian SNR	Gaussian MSE
SSM11	24.70	22.15	220.21
SSM19	24.45	18.47	233.41
SSM28	31.28	27.11	48.41
SSM34	25.94	20.50	165.59
SSM42	27.59	22.24	113.23

The statistical report is drawn between the noise image parameter and the Gaussian image parameter from Tables 1 and 2. This describes the pictorial representation of variation in pixel values or improvement or enhancement in image pixels. A comparative statistical report is shown in Fig. 5. The variations of pixels after adding noise are compared after removing noise using a Gaussian filter. The report briefly describes MSE, SNR, and PSNR of image quality performance measures. By this measurement, the better enhancement of the image for segmentation is visualized.

The first stage of the skin lesion segmentation algorithm is to learn representative texture distributions and calculate each distribution's texture distinctiveness metric. For each pixel in the image, a texture vector is extracted. Now, a new mask image is created with the same row and column values as the input image. The outer layer of the image is masked completely by filling with black color, where the inner part is white color with a length and height of 100 pixels from the center of the mask image. After creating the gray image and mask image, the segmentation is initiated by comparing both images and finding the contour image. The gray image is now enlarged into a double matrix, and the mask image is in the form of black and white, which is transformed by Euclidean distance to calculate the distance between each pixel and to nearest non-zero pixel.

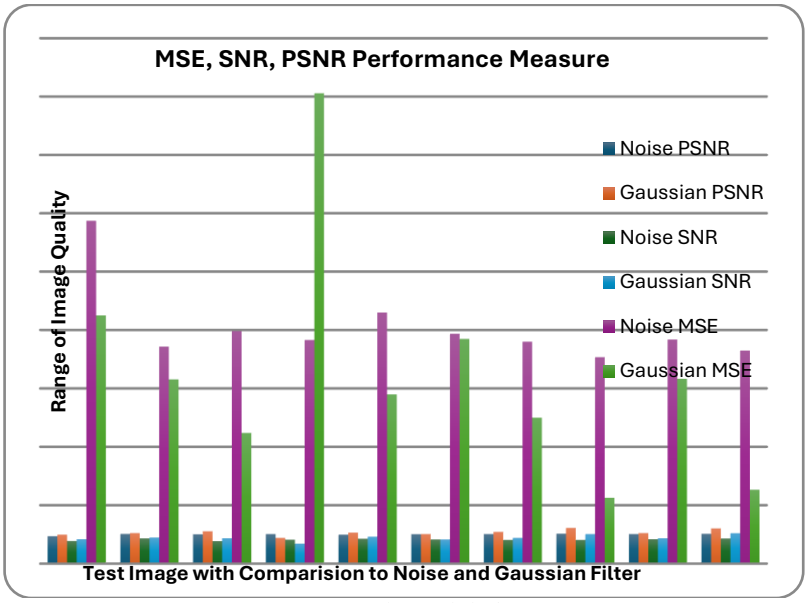

Fig. 5: Comparative Statistical Report.

The graphical comparison (see figure. 5) of three important quality image measures of noisy image MSE (Mean squared error), SNR (Signal noise ratio), and PSNR (Peak signal noise ratio) versus the parameter (SSM11, SSM19, SSM28, SSM34, and SSM42), indicate that the quality of the Gaussian filtered image is better than the quality of noisy image. The metric value of before and after a particular sample is depicted in the bar.

In this way, when applied to SSM28, the MSE drops considerably to 48.41, whereas the PSNR grows to 31.28 and the SNR rises to 27.11. The trend is replicated in most of the samples, and therefore it supports the argument that the Gaussian filter is effective in removing noise. These improvements are necessary because the methods can directly impact the contour segmentation quality, and the algorithm can identify the borders of the lesions better by maintaining important pixel-wise information and eliminating noise at the same time. Figure 5, in turn, qualifies as a quantitative verification of the pre-processing stage, which adds to the predictability of further segmentation procedures.

After identifying the distance of a nonzero pixel, the segmentation process is started by masking the curve over interior and exterior points on a grayscale image. Each point is shifted right, left, down, and up after comparing with non-zero pixels. The non-zero pixels derive the intensity values to find out perfect border in varying intensity values. On comparing each pixel point, if it varies in intensity value from its neighborhood, a small border is marked. After deriving the perfect border, the contour formed is shown in Fig. 6.

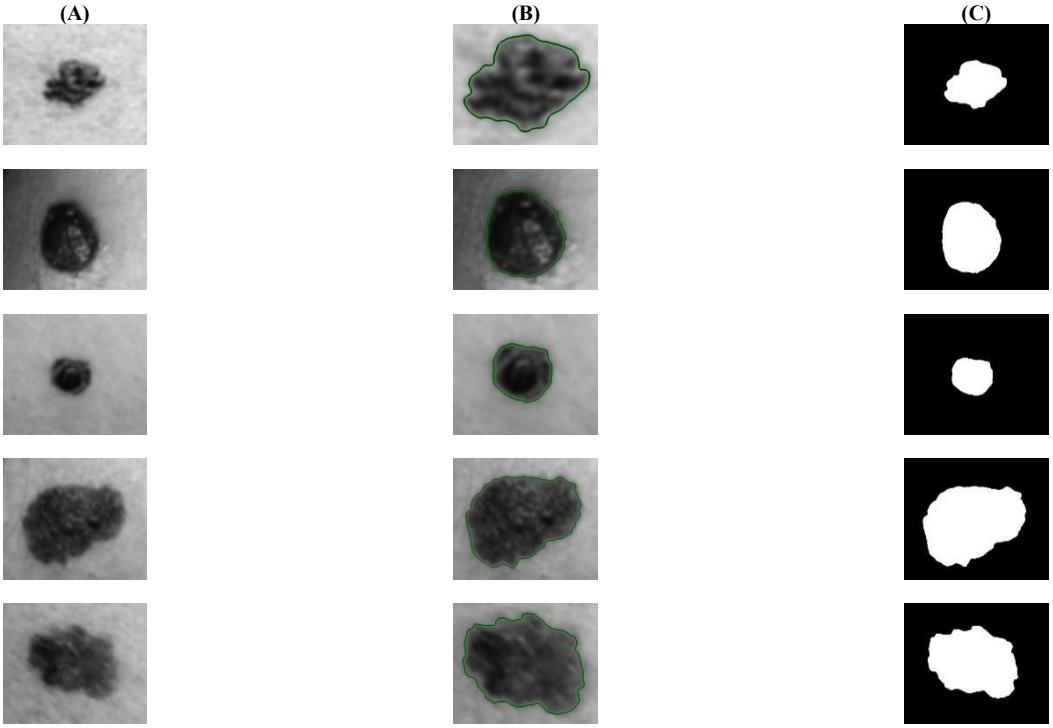

Fig. 6: Identifying Border from Masking Image to Segment Contour a) Masking b) Border Identification c) Segmented Image.

4.2. Performance metrics

After perfect segmentation, the segmented contour image is compared with the ground truth image to describe the performance measure of segmentation. After Iterative Contour segmentation, the performance measure of the DermQuest dataset is shown in Table 3.

Table 3: Performance Measure of DermQuest

Performances	SSM11	SSM19	SSM28	SSM34	SSM42
Accuracy (%)	93.27	93.43	98.70	90.71	91.06
Dice	77.16	82.90	91.58	86.45	85.94
Jaccard Index (%)	62.82	70.80	84.47	76.14	75.34
Sensitivity (%)	99.60	83.66	98.84	85.17	99.44
Specificity (%)	92.45	95.73	98.69	93.67	87.89
Error Rate (%)	06.73	06.57	01.30	09.29	08.94

After Iterative Contour segmentation, the performance measure of the DermQuest dataset is shown in Table 3.

Table 4: Performance Measure of DermIS

Performances	NM1	SSM14	SSM22	SSM29	SSM32
Accuracy (%)	93.59	88.82	92.57	95.26	93.47
Dice	89.42	76.93	68.55	89.62	85.66
Jaccard Index (%)	80.86	62.50	52.15	81.20	74.92
Sensitivity (%)	82.99	67.02	67.90	81.56	76.43
Specificity (%)	98.73	97.22	95.91	99.85	99.31
Error Rate (%)	06.41	11.18	07.43	04.74	06.53

On analyzing the performance measures of both datasets, the accuracy, sensitivity, and specificity are compared with the previous work to enhance the accuracy of the proposed work shown in Table 5.

Table 5: Comparison of Existing Accuracy with Proposed Accuracy Value

Method	Average Accuracy
FCMNN [8]	92.00%
SANN [9]	67.77%
SVM [10]	74.00%
Leaving-One-Out [11]	81.00%
Jacobian [12]	72.00%
SVM + KFD + RVM [13]	85.00%
SVM + LDA [14]	82.50%
Receiver Operating Characteristics [15]	90.00%
Nonparametric Spatio-Temporal [16]	88.00%
Proposed Method	93.43%

4.3. Comparative analysis with existing techniques

The iterative contour-based segmentation model proposed satisfies conditions of high performance mainly because, besides region-based features, the model also considers boundary-based features when evolving the contour. In contrast to the relatively kernel/feature dependent (e.g., SVM, FCMNN), it is based on statistical differences in intensity and constraints on curvatures, making it yield a more precise

evolution of the contour to live close to lesion boundaries. It will reduce the risk of overfitting, and it will become more adaptable to different kinds of lesions and image conditions.
Also, though SANN or hybrid SVM+KFD techniques are effective in learning features, they need large labeled datasets and computational computations, which can be time-consuming in real-world clinical applications, due to the restrictive and time-wasting operations they involve. Our approach is simplistic, can be understood, and does not rely on training a model, which will work well in situations of limited resources.
There is a possibility that even early positioning of masks and soft edges of lesions help in our approach, and affect the quality of segmentation. Moreover, despite the higher accuracy on DermQuest and DermIS datasets, our approach should be tested on a more extensive and diverse dataset to generalize the results and apply them to a wider range of clinical situations.
Figure 5 presents a comparative graphical presentation of the quality indicators of the images among the noisy images and the Gauss-filtered images; i.e., the PSNR (Peak Signal-to-Noise Ratio), SNR (Signal-to-Noise Ratio), and also MSE (Mean Squared Error). Higher PSNR and SNR and lesser MSE represent that the Gaussian filter is an effective filter that contributes immensely to the improvement of image quality in that it eliminates noise without any significant alteration of important properties of the image. E.g., SSM28 has a significant improvement in PSNR by 25.39 to 31.28 and a corresponding reduced MSE of 187.88 to 48.41, showing an evident clarity of signal. Such improvements are important because distortion and noise have direct consequences on the accuracy of the contour-based segmentation. The increase in image quality results in intensity gradients needed and structural information necessary to determine the contour evolution to be clearer, and ultimately results in more accurate detection of the boundary of the lesion.

4.4. Feature extraction

The melanoma is in the form of asymmetrical. To identify the asymmetry, a line is drawn between the centroid of the lesion. The center of the line divides the binary image into two halves; if both halves are the same, it is symmetry, else asymmetry. The asymmetry feature is discussed to prove whether the given input image is melanoma or not.

4.4.1. Rotated and measure asymmetry

Usually, melanoma should be in the form of asymmetrical and with an uneven border. To obtain the perfect asymmetrical rate, the RGB image should be segmented to get the binary image. The mole and the melanoma are identified in the form of even circular shape. The melanoma borders are uneven in shape. To prove obtained image is a melanoma or mole. The segmented contour image should be duplicated and named as the secondary contour image. The secondary contour image should be rotated and compared with the segmented contour image to prove whether the segmented image is melanoma or not, as described in Figure 7.
Algorithm

```
def calculate_asymmetry_index(Segmented_Inputs):
 # Image Segmentation and Centering
 Image_Row, Image_Column = size(Segmented_Inputs)
 Image_Centroid = (Image_Row/2, Image_Column/2)

 # Image Center Calculation
 Image_Center = ((x1 + x2) / 2, (y1 + y2) / 2)

 # Translation Vector
 delta_xy = (Image_Center[0] - Image_Centroid[0], Image_Center[1] - Image_Centroid[1])

 # Apply translation to align the image
 Image_Aligned = translate(Segmented_Inputs, delta_xy)

 # Rotation of the aligned image by angle theta
 Image_Rotated = rotate(Image_Aligned, theta)

 # Identifying matching points between the aligned and rotated images
 Original_Points, Distorted_Points = images_overlap(Image_Aligned, Image_Rotated)

 # Compare matched points
 Matched_Points = compare_equal_points(Original_Points, Distorted_Points)

 # Total points in the image
 Total_Points = count(Original_Points)

 # Symmetry Percentage
 Symmetry_Points = (Matched_Points / Total_Points) * 100

 # Asymmetry Index Decision
 if Symmetry_Points >= 75:
 return "Symmetry"
 else:
 return "Asymmetry"
```

The input RGB image is converted into a segmented binary image by iterative contour. The iterative contour fetches boundaries of the skin lesion and converts them into a binary image, as shown in Figure 8a. The obtained binary image should be centered; if not, the centroid of the binary image is identified, and a small transformation or rotation is performed to keep the binary image centered. The secondary contour image of the centered image is generated with a slight rotation of 30 degrees shown in Figure 8 b. Now the rotated binary image is overlapped on the centered binary image, and the rotated binary image acts as the foreground image and the centered binary

image acts as the background image. On comparing the patches of the foreground and background image, the original points and the distorted points are identified as shown in Figure 8c.

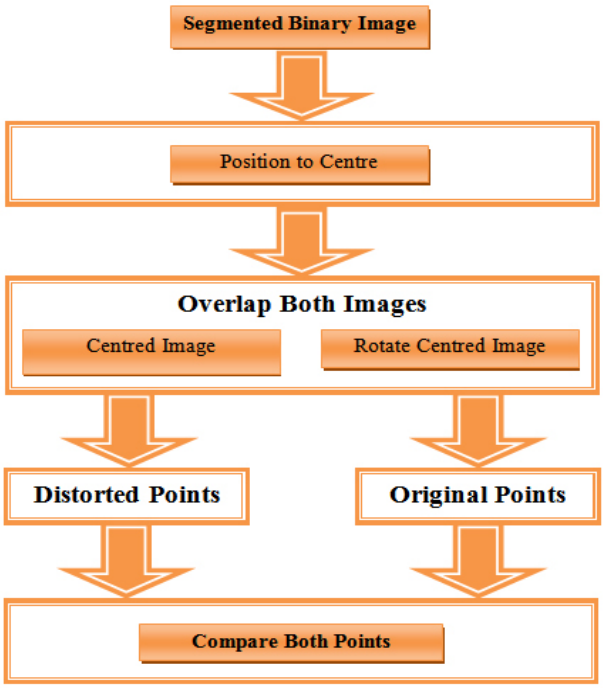

Fig. 7: Architecture Diagram of Rotated and Measure Asymmetry Feature Detection.

Original points are the number of white pixels in the background image. The distorted points are the number of unfit regions in which red and blue regions occurred while comparing both images, as shown in Figure 8d. If the distorted points are more than 80% then it is melanoma; if not, it is a mole.

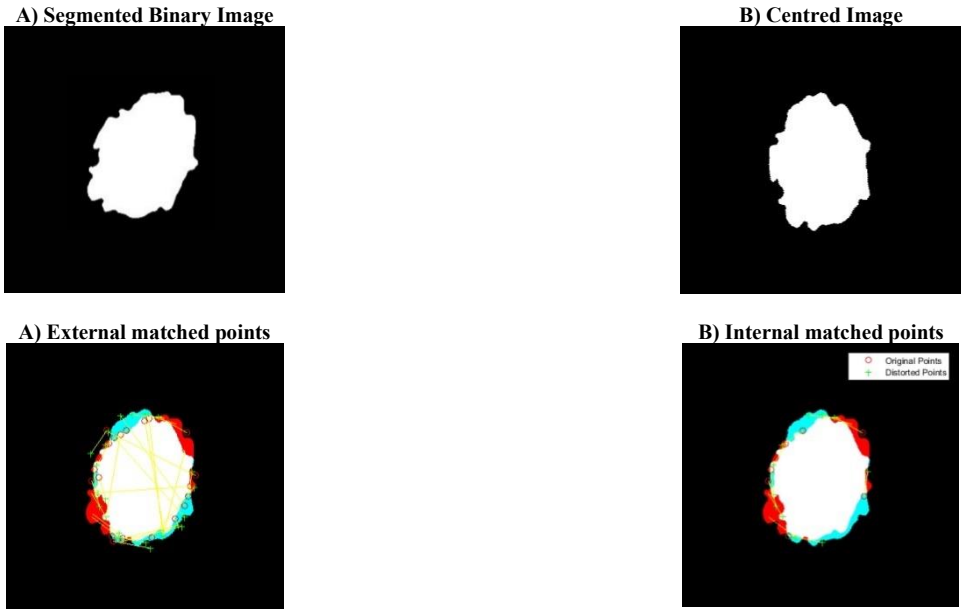

Fig. 8: Find Matched Points by Overlapping Centered Image and Rotated Image.

4.4.2. Hybrid border feature

Melanoma borders will, in general, be lopsided and may have scalloped or depressed edges, while usual moles will be common and have smoother edges. The main aim in finding the border is to recognize the authenticity of the image and to determine whether it is melanoma or not. The outer layer or the boundary of the binary image should be noted perfectly because the difference between a mole and melanoma is only in the border region. If there is any deviation in the border, it can be easily assumed that it may be melanoma.

Algorithm (Border Recognition)
Input: Take RGB Image
Output: Irregular Border
1) Segregate the input RGB Image
Input_Image(k,l)←input image Segmentation
Segmented_Image(k,l)= 0.1140*Blue_Colour + 0.2489* Red_Colour + 0.5870* Green_Colour
Val=2

2) Finding the center of Segmented Image
[Image_Row, Image_Column]= Size (Segmented_Image (k,l))
Image_Centroid(c) = Image_Row/Val
Image_Centroid(d) = Image_Column/Val
Image_Center(c) = (c1+c2)/Val
Image_Center(d) = (d1+d2)/Val
∇cd={ { Image_Center(c) - Image_Centroid(c)},{ Image_Center(d) - Image_Centroid(d)} }
Transform Segmented_Image (k,l) using ∇cd to Image_Border(c,d)
3) Identify Border from Center
a) Border over Axis-X
PRight = Segmeted_Image_Perimeter(Line(Image_Border (Center(x)), Image_Border (Center(y)), Image_Border (Right(x)), True_Pixels(x)))
PLeft = Segmeted_Image_Perimeter(Line(Image_Border (Center(x)), Image_Border (Center(y)), Image_Border (Left(x)), True_Pixels(x)))
b) Border over Axis-Y
PTop = Segmeted_Image_Perimeter(Line(Image_Border (Center(x)), Image_Border (Center(y)), Image_Border (Top(y)), True_Pixels(y)))
PBottom = Segmeted_Image_Perimeter(Line(Image_Border (Center(x)), Image_Border (Center(y)), Image_Border (Bottom(y)), True_Pixels(y)))
4) Border Asymmetric Index:
Min_Radius= Min(PRight , PLeft , PTop, PBottom)
Draw_Circle(Center(x,y), Min_Radius)
Border_Asymmetry Index:
If Associate (Min_Circle, Binary_Image) = Border_Symmetry? Border_Asymmetry

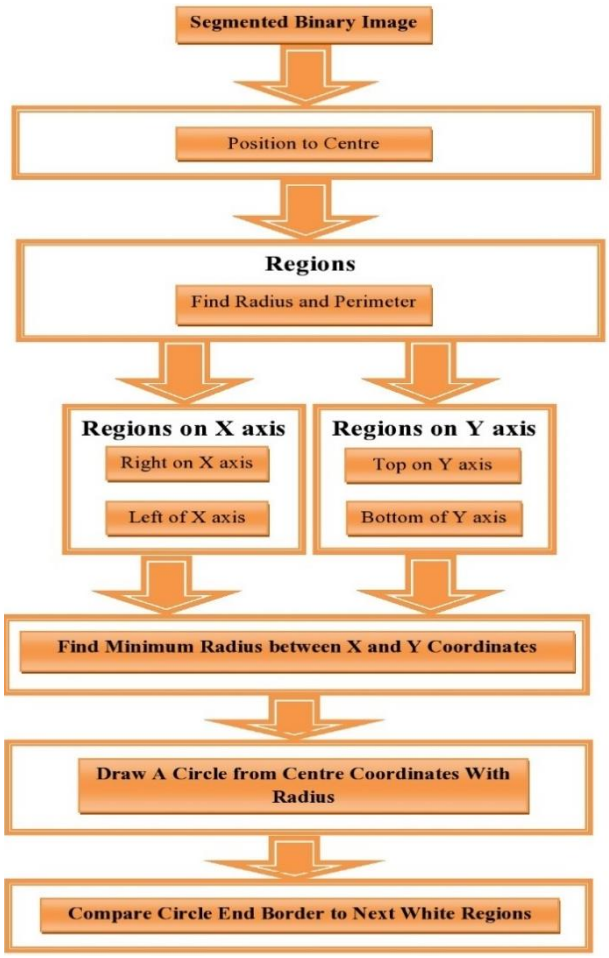

Fig. 9: Architecture Diagram for Circular Point Border Recognition.

The architecture diagram describes the working principle of the circular point edge detection methodology shown in Figure 9. After segmentation, the binary image is taken to find the boundary. Initially, the segmented binary image is translated to find the center point of the white pixels because the white region or true pixels are the infected region; that layer's boundary must be checked to differentiate.
After finding the center position in the binary image, the line is drawn from the center position to the right, left, top, and left regions. The minimum value of the line drawn between the centers to the bottom, left, top, and right is noted as the radius value. A circle is drawn from the center coordinates with a radius shown in Figure 10. The circle touches one edge of the binary image if all the edges of the circle and the boundary of the white pixels are the same; then it is a mole, if not, it is a melanoma.

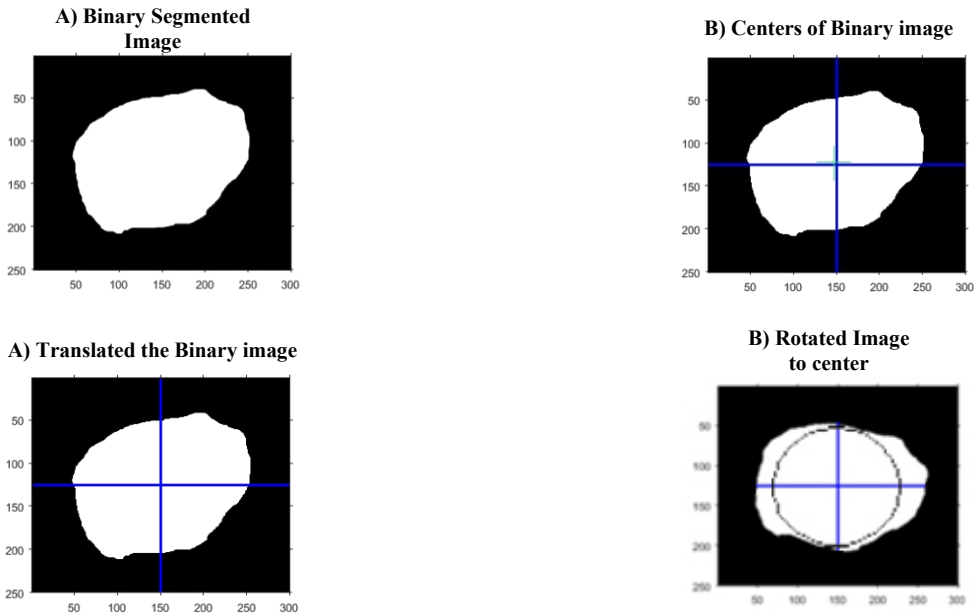

Fig. 10: Extract Border with Circular Point.

5. Discussion and future directions

The current study demonstrates the potential of traditional iterative contour segmentation and region-growing techniques in accurately delineating skin lesions from dermoscopy images. While the results are promising, several avenues for future research and development remain open to extend the clinical applicability and robustness of the method.

5.1. Testing on diverse and larger datasets

The proposed method was evaluated on the DermQuest and DermIS datasets. Future work should involve testing across ethnically and geographically diverse datasets, including images from underrepresented skin tones and rare lesion types, to evaluate the generalizability of the segmentation performance across population subgroups.

5.2. Real-time optimization

Although the method shows computational efficiency, there is scope to further optimize the implementation for real-time or embedded systems (e.g., mobile-based diagnostic tools). Techniques such as parallel contour updates or hardware-specific acceleration (e.g., FPGA/GPU) could reduce execution time and make the solution viable for point-of-care environments.

5.3. Integration with machine learning for feature extraction

Currently, features such as asymmetry and border irregularity are manually defined. Future enhancements may incorporate deep learning-based feature extraction or classification modules, allowing the system to automatically learn discriminative features from segmented regions. This could also enable risk scoring and severity grading of melanoma cases.

5.4. Robustness to imaging artifacts and illumination variance

Enhancements can be explored to address limitations in low-contrast or artifact-heavy images. Adaptive filtering methods, illumination normalization, and context-aware contour evolution could improve robustness under challenging imaging conditions.

5.5. Hybrid approaches

Future research could explore combining the current method with data-driven or semi-supervised models, enabling hybrid segmentation frameworks that leverage both algorithmic reliability and statistical learning from annotated examples. Addressing these directions can pave the way toward developing a more scalable, accurate, and intelligent diagnostic support tool that enhances early melanoma detection across various clinical settings.

6. Conclusion

The input RGB image is purged from clamor by the Gaussian channel, and the image is changed over in to cover image. With the assistance of Euclidean capacity, the outskirts are set apart from the focal point of ROI. Utilizing image slope, the progression of borderis is effectively recognized. The accuracy, sensitivity, and Specificity involve the proficiency of the portioned picture than the master's ground truth image. A normal accuracy pace of 93.43% and a normal sensitivity pace of 93.68% in the DermQuest dataset are acquired. A normal precision pace of 92.74% and a normal sensitivity pace of 98.20% in the DermIS dataset are acquired. The programmed division with shapes and locale development will be exceptionally valuable for dermatologists in recognizing injury territory. The component extraction, like asymmetry wellness, is separated to demonstrate whether the information of the dermoscopy image is melanoma or not.

6.1. Addressing research gaps and emerging trends

The suggested technique makes a relevant contribution to existing research gaps in the field of dermoscopic image analysis because it can deal with two challenging issues that have been mentioned repeatedly in the literature on the subject: the inhomogeneity of intensities and image noise. The old segmentation techniques lack precision in detecting the boundaries of the cases as well as variations in intensities that take place within the lesions. The method in this paper can capture boundaries in such inhomogeneous areas better because of the introduction of iterative contour evolution using regional statistics. Also, the combined Gaussian filtering is successful in eliminating salt-and-pepper noise, such as hair and sensor distortion effects, without suppressing the most important image characteristics. These design options are directly addressing the weaknesses identified in the past approaches and contributing to the increase in the trustworthiness of lesion segmentation.

Moreover, the work is consistent with other related trends in the strong focus on lightweight and explainable algorithms that can be deployed in real-time at the clinical or what could be an active-service setting, such as mobile. Subsequent research can be conducted with the hybridization of these traditional methods with the pre-processing or contrast enhancement modules based on deep learning to enhance segmentation further, even in extreme scenarios. Further generalisation to skin type and mechanisms of adaptive learning will be critical towards making the CAD systems in dermatology clinically ready.

62. Limitations and future work

Though the suggested idea reflects a high level of segmentation accuracy and good computational performance, it has a set of limitations to be taken into account. To begin with, Gaussian filtering is done in bringing out the salt-and-pepper noise, but the accuracy of this tool might fail in high-noise patterns or where the image has a complex artifact, e.g., hair occlusions or changes in lighting. Second, in images of the low contrast dermoscopy, the lesion borders are not highly distinguishable; it will be more challenging to make the contour evolution algorithm converge to the actual border. Third, differences in the pigmentation of the skin in various demographic groups have not been directly discussed, and this can impact the generalizability. Moreover, the present approach presupposes a relatively centered and isolated lesion that is not appear to be always true in clinical practice.

The work of the future will continue to refine the solution to influence robustness by the introduction of adaptive initialization, alteration of contrast enhancement methods, and evaluation on larger and ethnically diverse datasets. Integration of pre-processing or a hybrid approach based on machine learning could also further the versatility of the model to difficult image settings as well.

References

[1] Xu, S., Wang, Y., Zhao, Z., Peng, J., Cao, X., & Meng, D. (2023). Neural Gradient Regularizer. arXiv (Cornell University).

[2] Rodrigues, C. M., Boutry, N., & Najman, L. (2024). Transforming gradient-based techniques into interpretable methods. arXiv (Cornell University). https://doi.org/10.1016/j.patrec.2024.06.006.

[3] Abrahamyan, L., Truong, A. M., Philips, W., & Deligiannis, N. (2022). Gradient variance loss for Structure-Enhanced Image Super-Resolution. arXiv (Cornell University). https://doi.org/10.1109/ICASSP43922.2022.9747387.

[4] Y. Kim, B. -N. Kang and D. Kim, "Detector with focus: Normalizing gradient in image pyramid," 2017 IEEE International Conference on Image Processing (ICIP), Beijing, China, 2017, pp. 420-424, https://doi.org/10.1109/ICIP.2017.8296315.

[5] Deepak Gupta, Gowreesh Mago, Arnav Chavan, Dilip Prasad, Rajat Mani Thomas, "Pushing the Limits of Gradient Descent for Efficient Learning on Large Images," OpenReview.net, 2023.

[6] Liu, G., Liu, Q., Liang, J., & Sun, Q. (2023). Active contours driven by local and global intensity fitting energy with application to SAR image segmentation and its fast solvers. arXiv (Cornell University).

[7] Habis, A., Meas-Yedid, V., Angelini, E., & Olivo-Marin, J. (2024). Deep ContourFlow: Advancing Active Contours with Deep Learning. arXiv (Cornell University).

[8] Akbari, P., Ziaei, A., & Azarnoush, H. (2021). Deep active contours using locally controlled distance vector flow. arXiv (Cornell University).

[9] Bahl, G., Daniel, L., & Lafarge, F. (2022). SCR: Smooth Contour Regression with Geometric Priors. arXiv (Cornell University).

[10] Wang, D., Dang, X., Liu, W., & Wang, Y. (2023). Image segmentation using active contours with image structure adaptive gradient vector flow external force. Frontiers in Applied Mathematics and Statistics, 9. https://doi.org/10.3389/fams.2023.1271296.

[11] Turk, O., Acar, E., Irmak, E., Yilmaz, M., & Bakis, E. (2024). A Hybrid 2D Gaussian Filter and Deep Learning Approach with Visualization of Class Activation for Automatic Lung and Colon Cancer Diagnosis. Technology in Cancer Research & Treatment, 23. https://doi.org/10.1177/15330338241301297.

[12] Keilmann, A., Godehardt, M., Moghiseh, A., Redenbach, C., & Schladitz, K. (2024). Improved anisotropic gaussian filters. Image Analysis & Stereology, 43(1), 9–22. https://doi.org/10.5566/ias.3023.

[13] Zucchelli, E. M., & Jones, B. A. (2023). A Gaussian Integral Filter with Multivariate Laplace Process Noise. arXiv (Cornell University). https://doi.org/10.23919/FUSION52260.2023.10224147.

[14] Anand, S., & Sangeethapriya, G. (2020). Gaussian modulated hyperbolic tangent high pass filter for edge detection in noisy images. arXiv (Cornell University).

[15] Tang, W., Gong, Y., Liu, K., Liu, J., Pan, W., Liu, B., & Qiu, G. (2020). Gaussian Curvature filter on 3D meshes. arXiv (Cornell University).

[16] A. Soudani and E. Zagrouba, "Adaptive Region Based Active Contour Model for Image Segmentation," 2017 IEEE/ACS 14th International Conference on Computer Systems and Applications (AICCSA), Hammamet, Tunisia, 2017, pp. 717-724, https://doi.org/10.1109/AICCSA.2017.140.

[17] E. Iqbal, A. Niaz, A. A. Memon, U. Asim and K. N. Choi, "Saliency-Driven Active Contour Model for Image Segmentation," in IEEE Access, vol. 8, pp. 208978-208991, 2020, https://doi.org/10.1109/ACCESS.2020.3038945.

[18] S. Biswas, R. Hazra and S. Prasad, "A Region-based Level Set Formulation Using Machine Learning Approach in Medical Image Segmentation," TENCON 2019 - 2019 IEEE Region 10 Conference (TENCON), Kochi, India, 2019, pp. 470-475, https://doi.org/10.1109/TENCON.2019.8929350.

[19] X. Yang, X. Jiang, L. Zhou, Y. Wang and Y. Zhang, "Active Contours Driven by Local and Global Region-Based Information for Image Segmentation," in IEEE Access, vol. 8, pp. 6460-6470, 2020, https://doi.org/10.1109/ACCESS.2019.2963435.

[20] Chen, D., Mirebeau, JM., Shu, H. et al. A Region-Based Randers Geodesic Approach for Image Segmentation. Int J Comput Vis 132, 349–391 (2024). https://doi.org/10.1007/s11263-023-01881-z.

[21] A. Priya, R. K. Agrawal and B. Rana, "Fusion-based Multilevel Thresholding For Image Segmentation Using Evolutionary Algorithm," 2022 IEEE 9th Uttar Pradesh Section International Conference on Electrical, Electronics and Computer Engineering (UPCON), Prayagraj, India, 2022, pp. 1-7, https://doi.org/10.1109/UPCON56432.2022.9986438.

[22] S. Gao, X. Wang and C. Jin, "Analysis of Multi-Threshold Image Segmentation Method Based on Improved Sparrow Search Algorithm," 2022 4th International Conference on Applied Machine Learning (ICAML), Changsha, China, 2022, pp. 96-100, https://doi.org/10.1109/ICAML57167.2022.00025.
[23] Salaou, M. S. C., Conze, P., Kalti, K., Solaiman, B., & Mahjoub, M. A. (2017). Adaptive strategy for superpixel-based region-growing image segmentation. Journal of Electronic Imaging, 26(06), 1. https://doi.org/10.1117/1.JEI.26.6.061605.
[24] Shimodaira, H. (2017). Automatic color image segmentation using a square elemental Region-Based seeded region growing and merging method. arXiv (Cornell University).
[25] Dias, P. A., & Medeiros, H. (2020). Probabilistic semantic segmentation refinement by Monte Carlo region growing. arXiv (Cornell University). https://doi.org/10.1007/978-3-030-20890-5_9.
[26] Lagergren, J., Rutter, E., & Flores, K. (2020). Region Growing with Convolutional Neural Networks for Biomedical Image Segmentation. arXiv (Cornell University).
[27] Melekhov, I., Kannala, J., & Rahtu, E. (2017). Image Patch Matching Using Convolutional Descriptors with Euclidean Distance. arXiv (Cornell University). https://doi.org/10.1007/978-3-319-54526-4_46.
[28] Strutz, T. (2021). The Distance Transform and its Computation. arXiv (Cornell University).
[29] Fuseiller, G., Marie, R., Mourioux, G., Duno, E., & Labbani-Igbida, O. (2022). Enhancing distance transform computation by leveraging the discrete nature of images. Journal of Real-Time Image Processing, 19(4), 763–773. https://doi.org/10.1007/s11554-022-01221-3.
[30] Jourlin, M. (2024). Image Enhancement Thanks to Negative Grey Levels in the Logarithmic Image Processing Framework. Sensors, 24(15), 4969. https://doi.org/10.3390/s24154969.
[31] Jang, J., Lee, I., Kim, M., & Joo, K. (2024). AISDF: Structure-Aware Neural signed distance fields in indoor scenes. IEEE Robotics and Automation Letters, 9(5), 4106–4113. https://doi.org/10.1109/LRA.2024.3375117.
[32] Y. Chen, Y. Huang, L. Wang, H. Huang, J. Song, C. Yu, and Y. Xu, "Salt and Pepper Noise Removal Method Based on Stationary Framelet Transform with Non-Convex Sparsity Regularization," arXiv preprint arXiv:2110.09113, Oct. 2021. https://doi.org/10.1049/ipr2.12451.
[33] V. Singh, P. Agrawal, T. Sharma, and N. K. Verma, "Improved Adaptive Type-2 Fuzzy Filter with Exclusively Two Fuzzy Membership Function for Filtering Salt and Pepper Noise," arXiv preprint arXiv:2008.04114, Aug. 2020.
[34] A. A. Rafiee and M. Farhang, "A Deep Convolutional Neural Network for Salt-and-Pepper Noise Removal Using Selective Convolutional Blocks," arXiv preprint arXiv:2302.05435, Feb. 2023. https://doi.org/10.2139/ssrn.4373907.
[35] H. Dong, J. Yu, and C. Xiao, "Dual Reweighted Lp-Norm Minimization for Salt-and-Pepper Noise Removal," arXiv preprint arXiv:1811.09173, Nov. 2018.
[36] F. P. Loss et al., "Skin Cancer Diagnosis Using NIR Spectroscopy Data of Skin Lesions In Vivo Using Machine Learning Algorithms," arXiv preprint arXiv:2401.01200, Jan. 2024.
[37] D. N. T. Le et al., "Transfer Learning with Class-Weighted and Focal Loss Function for Automatic Skin Cancer Classification," arXiv preprint arXiv:2009.05977, Sep. 2020.
[38] S. Innani et al., "Deep Learning Based Novel Cascaded Approach for Skin Lesion Analysis," arXiv preprint arXiv:2301.06226, Jan. 2023. https://doi.org/10.1007/978-3-031-31407-0_46.
[39] A. A. Rafiee and M. Farhang, "An Automated and Interpretable Computer-Aided Approach for Skin Cancer Diagnosis Using Genetic Programming," IEEE Access, vol. 11, pp. 10679181, 2023.
[40] Le, D. N. T., et al. (2020). Transfer Learning with Class-Weighted and Focal Loss Function for Automatic Skin Cancer Classification. arXiv preprint arXiv:2009.05977.
[41] Innani, S., et al. (2023). Deep Learning Based Novel Cascaded Approach for Skin Lesion Analysis. arXiv preprint arXiv:2301.06226. https://doi.org/10.1007/978-3-031-31407-0_46.
[42] Loss, F. P., et al. (2024). Skin Cancer Diagnosis Using NIR Spectroscopy Data of Skin Lesions In Vivo Using Machine Learning Algorithms. arXiv preprint arXiv:2401.01200.